2012

Binary scattering model for Lennard-Jones potential: Transport coefficients and collision integrals for non-equilibrium gas flow simulations

Ayyaswamy Venkattraman
Purdue University

Alina A. Alexeenko
Purdue University - Main Campus, alexeenk@purdue.edu

Binary scattering model for Lennard-Jones potential: Transport coefficients and collision integrals for non-equilibrium gas flow simulations

Ayyaswamy Venkattraman and Alina A. Alexeenko[a)]
School of Aeronautics and Astronautics, Purdue University, West Lafayette, Indiana 47907, USA

(Received 8 September 2011; accepted 9 January 2012; published online 14 February 2012)

A Lennard-Jones (LJ) binary interaction model for dilute gases is obtained by representing the exact scattering angle as a polynomial expansion in non-dimensional collision variables. Rigorous theoretical verification of the model is performed by comparison with exact values of diffusion and viscosity cross sections and related collision integrals. The collision quantities given by the polynomial approximation model agree within 3.5% with those of the exact LJ scattering. The proposed model is compared in detail with the generalized soft sphere (GSS) model which is the closest in terms of fidelity among existing direct simulation Monte Carlo collision models. The GSS model's performance for the collision integral used in the first approximate of viscosity coefficient is comparable to the proposed model for most reduced temperatures. However, other collision integrals deviate significantly, even at moderate reduced temperatures. The high fidelity of the proposed model at low reduced temperatures enables non-equilibrium simulations of gases with deep LJ potential well such as metallic vapors. The model is based on the scattering angle as opposed to viscosity or diffusion coefficients and provides a direct link to molecular dynamics simulations.
 [http://dx.doi.org/10.1063/1.3682375]

I. INTRODUCTION

Non-equilibrium rarefied flows such as rapid expansions to vacuum, shock waves, and gas flows in microsystems require analyses based on the molecular description of gases due to the breakdown of continuum hypothesis. The Boltzmann equation is the governing equation for these flows and can be solved statistically using the direct simulation Monte Carlo (DSMC) (Ref. 1) method or deterministically by a discrete velocity method.[2–5] Transport in gases is completely determined by molecular properties such as the intermolecular potential and molecular mass which constitute the molecular model required for the solution of the Boltzmann equation. Molecular models with purely repulsive interaction such as the hard sphere[6] or the Maxwell molecules[1] lead to mathematical simplifications that provide certain advantages in solving the Boltzmann equation using discrete velocity methods and hence are widely used. The most popular molecular models used in the DSMC technique such as the variable hard sphere (VHS),[1] variable soft sphere,[7] generalized hard sphere,[8] generalized soft sphere (GSS) (Ref. 9) also correspond to purely repulsive interactions. All of these models involve parameters based on temperature variation of bulk transport properties such as viscosity and diffusion coefficients. In real gases, the long-range forces between molecules are attractive due to the dipole-dipole interaction. The repulsive-attractive force between most non-polar molecules for a wide range of relative energies is often described by the Lennard-Jones (LJ) (Ref. 10)

a)Electronic mail: alexeenk@purdue.edu.

potential:

$$U(r) = 4\epsilon_{\mathrm{LJ}}\left[\left(\frac{\sigma_{\mathrm{LJ}}}{r}\right)^{12} - \left(\frac{\sigma_{\mathrm{LJ}}}{r}\right)^{6}\right], \tag{1}$$

where ϵ_{LJ} is the potential well depth and σ_{LJ} corresponds to the distance at which the potential energy becomes zero. The potential well depth of a particular gas species determines the importance of the attractive component of the force. While LJ potential parameters based on a quantum mechanically constructed potential energy surface are likely to be the most accurate, certain empirical relations can be used for estimating LJ potential parameters using solid state properties and are given by[11]

$$\sigma_{\mathrm{LJ}} = 1.222\ \ V_{\mathrm{m,sol}}^{1/3}, \tag{2}$$

$$\epsilon_{\mathrm{LJ}} = 1.92\ \ kT_m, \tag{3}$$

where T_m is the melting temperature in K, k is the Boltzmann's constant, and $V_{\mathrm{m,\,sol}}$ is the solid state molar volume in $\mathrm{cm}^3/\mathrm{mol}$. For common gases, such as nitrogen and argon, which have relatively shallow potential well ($\epsilon_{\mathrm{LJ}} \leq 100$ K), the attractive component becomes important at low temperature conditions often encountered in, for example, supersonic flow experiments.[12–14]

On the other hand, for gases with deeper potential wells ($\epsilon_{\mathrm{LJ}} \geq 500$ K), such as metallic vapors, the attractive component of the intermolecular force is important even at temperatures of around 1000 K. Such metallic vapor flows are ubiquitous in material processing, for example, low-pressure vapor deposition of thin film materials.[15,16] In these applications, the actual energy distribution of molecules becomes important since the energy distribution of the vapor phase atoms arriving at the substrate determines the grain structure of the film. The energy distribution can be reproduced only by a collision model that captures the collision dynamics in detail as in the case of the LJ potential. The need to accurately describe these non-equilibrium gas flows motivates the development of high fidelity repulsive-attractive molecular interaction models for solution of the Boltzmann equation. Hence, the main goal of this paper is to verify a compact formulation of LJ binary scattering for non-equilibrium flow simulations by computing the corresponding collision cross sections and integrals as well as transport coefficients.

Recently, there has been increased interest in using realistic repulsive-attractive intermolecular potentials in discrete velocity methods.[17,18] In a recent work,[19] we proposed an efficient method to use the LJ intermolecular potential in DSMC simulations by obtaining the LJ scattering angle as a polynomial expansion in the non-dimensional collision parameters. The model is briefly discussed and summarized in Sec. III. The model was applied to DSMC simulations of a one-dimensional Couette flow thereby showing that the DSMC simulations reproduce the temperature variation of viscosity for the LJ potential. The method was also shown to be efficient with a computational cost that was comparable to the VHS model. The main objectives of the current work are to perform and present rigorous theoretical verification of the LJ polynomial approximation (LJPA) model by computing the various collision integrals defined by Chapman and Cowling[20] and comparing the results with the exact values obtained in this work as well as those reported in the past.[10,18] In particular, we present a detailed comparison between the LJPA model and the GSS model which is the purely repulsive DSMC collision model known to reproduce LJ viscosity variation. The viscosity and self-diffusion coefficients predicted by the proposed LJPA model are compared with those of purely repulsive models and also with experimental data.

An accurate and efficient LJ scattering model in DSMC is important for hybrid molecular dynamics (MD)/DSMC simulations. Since the MD interaction is often based on the LJ potential, the use of a LJ scattering model in the DSMC region of these hybrid simulations would ensure better compatibility at the interface than using purely repulsive interaction models. The atomistic simulation using hybrid DSMC/MD method by Gu *et al.*[21] used a modified form of the GSS model referred to as the MGSS model. The total cross section of the original GSS model is given by

$$\sigma_T = \sigma_{\mathrm{LJ}}^2(3.962\epsilon^{*-0.133} + 4.558\epsilon^{*-1.25}). \tag{4}$$

It can be noticed that the value of σ_T rapidly diverges for low values of reduced energies ($\epsilon^* \to 0$). The MGSS model essentially removes the singularity in the GSS total cross section by modifying σ_T for collision energies less than a certain cut-off value. However, the modification does not ensure the reproduction of all collision integrals of the LJ potential as was shown by Kim *et al.*,[22] and the LJ formulation proposed in this work can be used in such hybrid simulations such that all collision integrals of the LJ potential are reproduced within a certain tolerance. Valentini and Schwartzentruber[23] presented a comparison between MD simulations using the LJ potential and DSMC simulations using the VHS model for the structure of a normal shock wave and observed significant differences in the nature of the velocity distribution function within the shock wave obtained using the two methods, thereby showing that models based on transport coefficients cannot reproduce the velocity distribution of molecules though they can reproduce macroscopic properties such as density and temperature. Capturing the velocity and energy distributions accurately is important, for example, for thin film deposition modeling as outlined earlier.

The remainder of the paper is organized as follows. Section II presents the theory and the necessary background and Sec. III describes the polynomial approximation for the scattering angle and the numerical integration schemes used to compute the collision integrals. Section IV presents the results for the collision integrals of the LJPA model, compares the results with those of the GSS model and exact LJ scattering, and quantifies the accuracy of the LJPA model. Section V summarizes the conclusions.

II. THEORY AND BACKGROUND

The outcome of a binary elastic collision between two molecules for a given interaction potential is completely determined by the relative energy of the two colliding molecules ($\epsilon = m_r c_r^2/2$) and the trajectory-dependent impact parameter (b). Here, m_r is the reduced mass of the colliding molecules of mass m_1 and m_2 given by $m_r = m_1 m_2/(m_1 + m_2)$ and c_r is the relative velocity. Non-dimensional collision parameters can be defined as $b^* = b/\sigma_{\mathrm{LJ}}$ and $\epsilon^* = \epsilon/\epsilon_{\mathrm{LJ}}$ and are referred to as reduced impact parameter and reduced collision energy, respectively. For a binary collision between molecules interacting through a LJ potential, the scattering angle χ is computed using the expression[24]

$$\chi = \pi - 2\sqrt{1 + cz - (1+c)z^2} \int_0^1 \{1 - [1 + cz - (1+c)z^2]u^2 + czu^6 - (1+c)z^2u^{12}\}^{-1/2} du, \tag{5}$$

where $c = (2/\epsilon^*)[1 + \sqrt{1+\epsilon^*}]$, $z = (4/c\epsilon^*)(\sigma_{\mathrm{LJ}}/r_0)^6$, and $u = r_0/r$ where r_0 is the distance of closest approach between the two molecules. Varying u from 0 to 1 varies r from ∞ to r_0. The parameter z in the above integral depends on b^* and ϵ^* and is obtained by solving the implicit equation

$$b^* = \left(\frac{4}{c\epsilon^*}\right)^{1/6} \sqrt{1 + cz - (1+c)z^2}\, z^{-1/6}. \tag{6}$$

It should be mentioned that the integral in Eq. (5) cannot be computed analytically and requires numerical integration using techniques such as those described in Sec. III.

The expression for χ in Eq. (5) is in terms of reduced collision parameters b^* and ϵ^* and is applicable to an arbitrary gas. However, for a given value of the relative kinetic energy, the value of ϵ^* depends on the potential well depth ϵ_{LJ} which shows a strong dependence on the gas under consideration. The relative kinetic energy of colliding molecules is a monotonically increasing function of the macroscopic temperature of the gas. Therefore, the importance of the attractive component of the intermolecular force depends on the flow conditions such as temperature as well as the LJ potential parameters of the gas, in particular, ϵ_{LJ}. Table I summarizes the LJ parameters of various gas species from published data.[25] For aluminum, gold, and copper vapors, the empirical relations suggested by Bird *et al.*[11] are used. The LJ parameters for copper vapor in Table I were obtained using $T_m = 1358$ K and $V_{\mathrm{m,\,sol}} = 7.103$ cm^3/mol. For gold, the corresponding values were $T_m = 1337$ K and $V_{\mathrm{m,\,sol}} = 10.207$ cm^3/mol. For aluminum, $T_m = 933.5$ K and $V_{\mathrm{m,\,sol}} = 10.0$ cm^3/mol. It should also be mentioned that water being a polar molecule is better represented

TABLE I. Comparison of Lennard-Jones potential parameters and mean reduced relative energy at 1000 K for various gases.

Gas	ϵ_{LJ}/k (K)	σ_{LJ} (nm)	ϵ^* at 1000 K
Helium, He	10.22	0.2576	173.6
Hydrogen, H_2	33.3	0.2968	55.0
Nitrogen, N_2	91.5	0.3681	19.2
Oxygen, O_2	113	0.3433	15.3
Argon, Ar	124	0.3045	13.6
Methane, CH_4	137	0.3822	12.1
Carbon dioxide, CO_2	190	0.3996	8.3
Nitrous Oxide, N_2O	220	0.3879	7.1
Water vapor, H_2O	230.9	0.2824	6.5
Aluminum vapor, Al	1792.3	0.2633	0.84
Gold vapor, Au	2567	0.2651	0.58
Copper vapor, Cu	2600	0.2349	0.6

by an additional attractive term as given by the Stockmayer potential.[9] The shallow potential well for helium implies that the attractive component of force is not very important. The importance of the attractive component increases with increasing ϵ_{LJ}. Note the extremely large values of ϵ_{LJ} for metallic vapors. Table I also shows the estimated mean reduced collision energy,[1] ϵ^*, in equilibrium at a temperature of 1000 K. The estimate is based on a VHS gas and is given by $\epsilon^* = (2.5 - \omega)kT/\epsilon_{LJ}$ where ω is the viscosity-temperature exponent. While ω for the common gases was taken from Bird,[1] the ω for copper was taken from Venkattraman and Alexeenko.[26] The ω for Al and Au were taken as 1.0 due to lack of data. Typically, the attractive component of the force is important for temperatures corresponding to $\epsilon^* \leq 2$. Based on Table I, such conditions occur for metallic vapor flows even at high temperatures and such flows are likely to require a formulation of the LJ molecular interaction to completely describe the relevant physics.

III. MODEL DESCRIPTION AND NUMERICAL APPROACH

A. Direct computation and polynomial expansion of scattering angle

Here, we describe the numerical integration procedure used to evaluate χ given by Eq. (5). For a given value of b^* and ϵ^*, Eq. (6) is solved using a bisection method and the solution for z is used to compute χ by numerical integration of Eq. (5). The numerical integration is performed using the Gauss-Chebyshev quadrature method. The integral in Eq. (5) is written as

$$\int_0^1 I(u)du = \sum_{k=0}^{M-1} \frac{1}{2} w_k I\left(\frac{y_k + 1}{2}\right)\sqrt{1 - y_k^2}, \tag{7}$$

where w_k are the weights for Gauss-Chebyshev quadrature, y_k are the zeros of the Mth degree Chebyshev polynomial ϕ_M, and I is the integrand in Eq. (5) given by

$$I(u) = \{1 - [1 + cz - (1 + c)z^2]u^2 + czu^6 - (1 + c)z^2u^{12}\}^{-1/2}. \tag{8}$$

The zeros, y_k, of ϕ_M are given by

$$y_k = \cos\left(\frac{(2k + 1)\pi}{2M}\right) \tag{9}$$

and the weights are all equal and are given by

$$w_k = \frac{\pi}{M}. \tag{10}$$

For results presented in this work, the value of M was used as 800 with further increase in the number of quadrature points leading to negligible difference in the computed value of χ including regions

near the singularity due to orbiting[10,18] collisions. It should be mentioned that any other numerical integration scheme such as Gauss-Legendre could have been used and would have given the same result as long as sufficient number of points was used.

The value of scattering angle χ is the only parameter on which the collision integrals and hence the transport coefficients depend. Following a convention similar to that of Hirschfelder *et al.*,[10] the reduced collision cross sections, $S^{(l)}(\epsilon^*)$, are given by

$$S^{(l)}(\epsilon^*) = \frac{4}{\left[2 - \frac{1+(-1)^l}{1+l}\right]} \int_0^\infty [1 - \cos^l \chi] b^* db^*. \tag{11}$$

The reduced collision cross section for viscosity corresponds to $l = 2$. For $l = 2$, the reduced collision cross section simplifies to

$$S^{(2)}(\epsilon^*) = 3 \int_0^\infty (1 - \cos^2 \chi) b^* db^*. \tag{12}$$

The collision integrals $W^{(l)}(n; x)$ are then obtained using $S^{(l)}(\epsilon^*)$ as

$$W^{(l)}(n; x) = \frac{1}{8}\left[2 - \frac{1 + (-1)^l}{1 + l}\right] x^{n+2} \int_0^\infty e^{-x\epsilon^*} \epsilon^{*n+1} S^{(l)}(\epsilon^*) d\epsilon^*, \tag{13}$$

where $x = \epsilon_{\mathrm{LJ}}/kT$. The first approximation of Chapman-Enskog viscosity[20] uses $l = 2$ and $n = 2$ and is given by

$$W^{(2)}(2; x) = \frac{1}{6} x^4 \int_0^\infty e^{-x\epsilon^*} \epsilon^{*3} S^{(2)}(\epsilon^*) d\epsilon^*. \tag{14}$$

Therefore, using the scattering angle computed by Gauss-Chebyshev numerical integration in the present work, the reduced collision cross section $S^{(2)}(\epsilon^*)$ and $W^{(2)}(2; x)$ can be computed using numerical integration techniques summarized later.

In our recent work,[19] we reported a representation of the LJ scattering angle, χ, in terms of a polynomial expansion in the reduced impact parameter, b^* and the reduced collision energy, ϵ^*. The main advantage of this representation, referred to, is its use in non-equilibrium flow simulations using methods such as the DSMC in which the scattering angle has to be computed for millions of collision events during the simulation. While the polynomial expansion was shown to reproduce the temperature variation of viscosity and thermal conductivity by performing DSMC simulations, it is important to compute the collision integrals and compare with the collision integrals obtained using the exact χ by numerical integration and also with those reported by Hirschfelder *et al.*[10] The LJPA model is briefly summarized below. The LJPA scattering angle is given in terms of b^* and ϵ^* as

$$\chi = \sum_{i=0}^{7} \sum_{j=0}^{7-i} \hat{\chi}_{ij} \hat{b}^{*i} \hat{\epsilon}^{*j}, \tag{15}$$

where $\hat{\chi}_{ij}$ are coefficients described later, $\hat{b}^*$ and $\hat{\epsilon}^*$ are given by transformations of the form

$$\hat{b}^* = \frac{2b^* - (b^*_{\min} + b^*_{\max})}{b^*_{\max} - b^*_{\min}}, \tag{16}$$

$$\hat{\epsilon}^* = \frac{2\epsilon^* - (\epsilon^*_{\min} + \epsilon^*_{\max})}{\epsilon^*_{\max} - \epsilon^*_{\min}} \tag{17}$$

with $b^*_{\min}$, $b^*_{\max}$, $\epsilon^*_{\min}$, and $\epsilon^*_{\max}$ depending on the domain under consideration. The six different domains with different values of coefficients $\hat{\chi}_{ij}$ in each domain are summarized below:

$$\text{Domain 1(non-glancing, slow)} : [0, 0.95\mathrm{b}^*_0(\epsilon^*)] \times [10^{-3}, 0.8], \tag{18}$$

$$\text{Domain 2(non-glancing, fast)} : [0, 0.98\mathrm{b}^*_0(\epsilon^*)] \times (0.8, 5], \tag{19}$$

TABLE II. Coefficients $\tilde{b}^*_{0i}$ for computing b^*_0 using Eq. (26).

i	0	1	2	3	4	5	6	7	8	9
$\tilde{b}^*_{0i}$	1.25024	−0.06106	−0.03244	0.15898	0.55705	−0.96732	−1.09018	1.60118	0.80013	−0.99571

$$\text{Domain 3(non-glancing, very fast)} : [0, 0.98\mathrm{b}^*_0(\epsilon^*)] \times (5, 20], \tag{20}$$

$$\text{Domain 4(glancing, slow)} : [1.05\mathrm{b}^*_0(\epsilon^*), \mathrm{B}^*(\epsilon^*)] \times [10^{-3}, 0.8], \tag{21}$$

$$\text{Domain 5(glancing, fast)} : [1.02\mathrm{b}^*_0(\epsilon^*), \mathrm{B}^*(\epsilon^*)] \times (0.8, 5], \tag{22}$$

$$\text{Domain 6(glancing, very fast)} : [1.02\mathrm{b}^*_0(\epsilon^*), \mathrm{B}^*(\epsilon^*)] \times (5, 20]. \tag{23}$$

In the above equations, b^*_0 is defined as follows. For values of $\epsilon^* \le 0.8$,

$$b^*_0 = \left(\frac{4}{c\epsilon^*}\right)^{1/6} \sqrt{1 + cz_0 - (1+c)z_0^2}\, z_0^{-1/6}, \tag{24}$$

where z_0 is the critical value of z given by[10]

$$z_0 = \frac{2}{5}\left[\frac{1 - \sqrt{1 - 5\epsilon^*/4}}{1 + \sqrt{1+\epsilon^*}}\right]. \tag{25}$$

For $0.8 < \epsilon^* \le 20$,

$$b^*_0 = \sum_{i=0}^{9} \tilde{b}^*_{0i} (2\epsilon^*/19.2 - 20.8/19.2)^i, \tag{26}$$

where $\tilde{b}^*_{0i}$ are given in Table II for $0 \le i \le 9$. In the definitions for the different domains, B^* is given by[7]

$$B^* = \max\left[\left(\frac{0.4\pi}{\epsilon^*}\right)^{1/6}, \left(\frac{0.6\pi}{\epsilon^*}\right)^{1/12}\right]. \tag{27}$$

Physically, using the above expression for B^* implies that collisions with scattering angle less than 0.1 radians are neglected. This will lead to a small deviation from the exact collision integrals and will be quantified in Sec. IV. The values of $\hat{b}^*$ and $\hat{\epsilon}^*$ are obtained from b^* and ϵ^* using Eqs. (16) and (17). The specific transformations for each domain are obtained by using the relevant $b^*_{\max}$, $b^*_{\min}$, $\epsilon^*_{\max}$, and $\epsilon^*_{\min}$. For example, the transformation for domain 1 would be

$$\hat{b}^* = \frac{2b^* - 0.95b^*_0(\epsilon^*)}{0.95b^*_0(\epsilon^*)}, \tag{28}$$

$$\hat{\epsilon}^* = \frac{2\epsilon^* - (0.8 + 0.001)}{0.8 - 0.001}. \tag{29}$$

The coefficients corresponding to a given domain, as tabulated in Tables III–VIII, are used in Eq. (15) to obtain the value of $\chi(b^*, \epsilon^*)$ for given collision parameters.

It can be observed that the six domains described above do not include $0.95b^*_0(\epsilon^*) < b^* < 1.05b^*_0(\epsilon^*)$ for $10^{-3} \le \epsilon^* \le 0.8$ and $0.98b^*_0(\epsilon^*) < b^* < 1.02b^*_0(\epsilon^*)$ for $0.8 < \epsilon^* \le 20.0$. While one option is to assume a certain constant value for these regions, it could lead to deviation of

TABLE III. Coefficients for computing χ in domain 1 (non-glancing, slow): $[0, 0.95b_0^*(\epsilon^*)] \times [0.001, 0.8]$.

	j							
i	0	1	2	3	4	5	6	7
0	1.38705	0.08519	− 0.02818	0.06121	0.05697	− 0.12524	− 0.06137	0.09912
1	− 1.97605	0.11570	− 0.02961	− 0.04771	0.05340	0.04660	− 0.05773	
2	− 0.60876	0.02900	− 0.00982	− 0.04166	0.01084	− 0.00130		
3	− 0.62908	0.02215	− 0.02141	0.03690	0.00992			
4	0.43094	0.02673	0.06866	0.05901				
5	0.74955	− 0.05907	0.06626					
6	− 0.81407	− 0.07607						
7	− 0.88752							

TABLE IV. Coefficients for computing χ in domain 2 (non-glancing, fast): $[0, 0.98b_0^*(\epsilon^*)] \times [0.8, 5.0]$.

	j							
i	0	1	2	3	4	5	6	7
0	1.62179	− 0.00111	− 0.14573	0.11133	0.08726	–0.01804	− 0.06260	0.00756
1	− 1.69670	0.30689	− 0.26357	− 0.29093	0.24040	0.18177	− 0.10923	
2	− 0.56380	0.59637	0.58157	− 0.61790	− 0.28065	0.23718		
3	− 0.68270	− 0.82651	1.06730	0.43978	− 0.40662			
4	0.26139	− 1.27015	− 0.63774	0.63216				
5	0.51337	0.81639	− 0.89707					
6	− 0.12700	0.97283						
7	− 0.13394							

TABLE V. Coefficients for computing χ in domain 3 (non-glancing, very fast): $[0, 0.98b_0^*(\epsilon^*)] \times [5.0, 20.0]$.

	j							
i	0	1	2	3	4	5	6	7
0	1.53514	− 0.04081	− 0.01009	− 0.01188	0.04477	− 0.00173	− 0.03650	0.01578
1	− 1.80199	− 0.08299	0.02086	− 0.02847	0.03209	0.02354	− 0.03079	
2	− 0.37454	− 0.10448	0.01727	0.00337	− 0.01291	− 0.00537		
3	− 0.31401	0.22851	− 0.03373	0.03273	− 0.00930			
4	0.08474	0.48647	− 0.05731	0.03146				
5	0.49546	− 0.08686	− 0.01689					
6	0.24943	− 0.29037						
7	− 0.03613							

TABLE VI. Coefficients for computing χ in domain 4 (glancing, slow): $[1.05b_0^*(\epsilon^*), B^*(\epsilon^*)] \times (0.001, 0.8]$.

	j							
i	0	1	2	3	4	5	6	7
0	− 0.22164	− 0.00513	− 0.00288	− 0.00255	0.00255	0.00335	− 0.00190	− 0.00206
1	0.18759	0.01517	0.00356	− 0.00264	− 0.00375	0.00308	0.00301	
2	− 0.11562	− 0.01521	0.00176	0.00338	− 0.00396	− 0.00338		
3	0.06791	0.00017	− 0.00307	0.00520	0.00380			
4	− 0.01384	0.00314	− 0.00759	− 0.00467				
5	0.00023	0.01350	0.00646					
6	− 0.03542	− 0.01095						
7	0.02614							

TABLE VII. Coefficients for computing χ in domain 5 (glancing, fast): $[1.02b_0^*(\epsilon^*), B^*(\epsilon^*)] \times (5.0, 20.0]$.

	j							
i	0	1	2	3	4	5	6	7
0	−0.25855	0.07903	0.13952	−0.17885	−0.29568	0.18264	0.17837	−0.05321
1	0.28657	−0.03989	−0.29706	−0.39385	0.56210	0.39476	−0.34398	
2	−0.21628	0.08245	−0.23342	0.56784	0.42132	−0.61386		
3	0.18752	−0.02691	0.22406	0.08013	−0.48026			
4	0.15210	−0.10932	−0.28712	0.04639				
5	−0.22832	−0.24377	0.36129					
6	−0.08788	0.22444						
7	0.08385							

TABLE VIII. Coefficients for computing χ in domain 6 (glancing, very fast): $[1.02b_0^*(\epsilon^*), B^*(\epsilon^*)] \times (5.0, 20.0]$.

	j							
i	0	1	2	3	4	5	6	7
0	−0.12606	0.04761	−0.01890	0.01449	−0.00714	−0.00415	0.00299	0.00015
1	0.04187	−0.04974	0.03353	−0.01731	0.01173	−0.00866	0.00073	
2	0.00003	0.00984	−0.01684	0.01111	−0.01798	0.01505		
3	−0.00545	−0.00071	0.00326	−0.00352	0.00773			
4	−0.00147	0.00056	0.01149	−0.00823				
5	0.00121	0.00814	−0.01027					
6	0.00217	−0.00389						
7	−0.00051							

transport properties since χ varies extremely rapidly in these regions ($10^{-3} \le \epsilon^* \le 1.0$). Therefore, we represent χ in these excluded regions as follows:

$$\chi(0.95b_0^* < b^* < b_0^*, 10^{-3} \le \epsilon^* \le 0.8) = \chi(0.95b_0^*, \epsilon^*)\left(\frac{0.05}{1 - b^*/b_0^*}\right)^{(-10b^*/b_0^* + 10.29)},$$

$$\chi(b_0^* < b^* < 1.05b_0^*, 10^{-3} \le \epsilon^* \le 0.8) = \chi(1.05b_0^*, \epsilon^*)\left(\frac{0.05}{b^*/b_0^* - 1}\right)^{(7b^*/b_0^* - 6.68)},$$

$$\chi(0.98b_0^* < b^* \le b_0^*, 0.8 < \epsilon^* \le 1.0) = \chi(0.98b_0^*, \epsilon^*)(b^* - 0.98b_0^*)^{-8(b^*/b_0^* - 0.98)},$$

$$\chi(b_0^* \le b^* < 1.02b_0^*, 0.8 < \epsilon^* \le 1.0) = \chi(1.02b_0^*, \epsilon^*)(1.02b_0^* - b^*)^{-8(1.02 - b^*/b_0^*)},$$

$$\chi(0.98b_0^* < b^* \le b_0^*, 1.0 < \epsilon^* \le 20.0) = \chi(0.98b_0^*, \epsilon^*),$$

$$\chi(b_0^* < b^* < 1.02b_0^*, 1.0 < \epsilon^* \le 20.0) = \chi(1.02b_0^*, \epsilon^*).$$

The model summarized above is very similar to that used to perform DSMC simulations in our recent work.[19] For the DSMC simulations, an approximation of χ for $\epsilon^* > 20$ was not required because the temperatures considered corresponded to reduced temperatures of $kT/\epsilon_{LJ} < 2.5$. However, in order to compute the collision integrals for a wide range of kT/ϵ_{LJ} values, the elastic scattering angle is required for $\epsilon^* > 20$. Also, even for low reduced temperatures, the integration limits ranging from 0 to ∞ requires an approximation of χ for $\epsilon^* > 20$. It should be mentioned that the influence of collisions corresponding to $\epsilon^* > 20$ will be negligible for $kT/\epsilon_{LJ} < 2.5$ and integrating from 0 to ∞ is purely for mathematical rigorousness. Therefore, a polynomial expansion was obtained for $20 < \epsilon^* \le 1000$ similar to the other polynomial expansions using the method detailed in our previous work.[19] The coefficients are tabulated in Table IX. For values of $\epsilon^* > 1000$ and $0 \le b^* \le 0.95B^*$, it was observed that the following simple expression is

TABLE IX. Coefficients for computing χ in domain 7: $[0, B^*(\epsilon^*)] \times (20.0, 1000.0]$.

	j							
i	0	1	2	3	4	5	6	7
0	1.52914	0.01788	−0.01224	0.02350	0.27840	−0.42807	−0.37884	0.50895
1	−1.74920	−0.03429	0.06886	0.03544	−0.05438	0.15834	−0.21535	
2	−0.29241	−0.03677	−0.26140	0.50657	0.24051	−0.40391		
3	−0.15554	0.07881	−0.17454	−0.21138	0.35612			
4	0.50800	−0.11878	0.08984	−0.13564				
5	0.68091	0.00851	−0.04815					
6	−0.14241	0.10519						
7	−0.30169							

a good approximation:

$$\chi = \pi \left(1 - \frac{b^*}{0.95B^*}\right). \tag{30}$$

For values of $\epsilon^* > 1000$ and $b^* > 0.95B^*$, the value of $\chi = 0$. It should be mentioned that for very high energy collisions, such as $\epsilon^* > 1000$, the accuracy of the LJ potential itself is questionable and the above linear approximation is purely for the purpose of integrating between the limits 0 and ∞. The values of collision integrals at moderate reduced temperatures $kT/\epsilon_{\mathrm{LJ}} \leq 100$ will not be affected by the form of χ for $\epsilon^* > 1000$. The scattering angles obtained using the LJPA model and using direct numerical integration agree within 10% (Ref. 19) except very close to the region of orbiting collisions where the approximate form of the LJPA model leads to larger errors. However, the collisions very close to the orbiting region form only a very small fraction of the total number of collisions. In order to compare the computational cost of obtaining χ using direct numerical integration with that of the LJPA model, the time taken to compute 10 000 values of χ for a wide range of b^* and ϵ^* was estimated for both methods. It was observed that the LJPA model required only 2.3 s in comparison to 334.22 s required using direct numerical integration.

B. Computation of collision integrals

In this section, we summarize the numerical integration procedures used to evaluate the collision integrals for the exact scattering angle and for the LJPA model. As described earlier, obtaining the collision integrals consists of the evaluation of $S^{(l)}(\epsilon^*)$ using Eq. (11) and then using it in Eq. (13) to compute $W^{(l)}(n; x)$ for given values of l, n, and x. In order to overcome the singularity at b_0^*, Eq. (11) is written as

$$S^{(l)}(\epsilon^*) = \frac{4}{\left[2 - \frac{1+(-1)^l}{1+l}\right]} \left(\int_0^{b_0^*} [1 - \cos^l \chi] b^* db^* + \int_{b_0^*}^{\infty} [1 - \cos^l \chi] b^* db^*\right). \tag{31}$$

The first integral in Eq. (31) is computed using Gauss-Chebychev quadrature similar to that used to compute the scattering angle, χ:

$$\int_0^{b_0^*} [1 - \cos^l \chi] b^* db^* = \sum_0^{M-1} \frac{b_0^*}{2} w_k (1 - \cos^l \chi) \frac{b_0^* y_k + b_0^*}{2} \sqrt{1 - y_k^2}, \tag{32}$$

where y_k are the zeros of the Mth degree Chebyshev polynomial and χ is evaluated at $((b_0^* y_k + b_0^*)/2, \epsilon^*)$. Since the integration limits are not finite for the second integral in Eq. (31), Gauss-Laguerre quadrature is used and the integral is computed as

$$\int_{b_0^*}^{\infty} [1 - \cos^l \chi] b^* db^* = \sum_{k=1}^{N_{LG}} w_{k,0,N_{LG}} [1 - \cos^l \chi] / e^{-z_{k,0,N_{LG}}}, \tag{33}$$

where $z_{k,0,N_{LG}}$ is the kth zero of the Laguerre polynomial[27] of degree N_{LG}, $L_{0,N_{LG}}$ and $w_{k,0,N_{LG}}$ is the corresponding weight. χ is evaluated at $(b_0^* + z_{k,0,N_{LG}}, \epsilon^*)$. The zeros of the Laguerre polynomials, unlike the Chebyshev polynomials, do not have a simple analytic representation. The weights are given by[27]

$$w_{k,0,N_{LG}} = \frac{1}{z_{k,0,N_{LG}}} \frac{1}{L'^2_{0,N_{LG}}(z_{k,0,N_{LG}})}. \tag{34}$$

The weights can be computed using standard functions in scientific computation software such as MATLAB and MATHEMATICA. For the integration in this work, the value of N_{LG} was fixed at 100.

For the LJPA model, the value of $\chi = 0$ for $b^* > B^*$ and therefore

$$S^{(l)}(\epsilon^*) = \frac{4}{\left[2 - \frac{1+(-1)^l}{1+l}\right]} \int_0^{B^*} [1 - \cos^l \chi] b^* db^* \tag{35}$$

which, to avoid the singularity, is written as

$$S^{(l)}(\epsilon^*) = \frac{4}{\left[2 - \frac{1+(-1)^l}{1+l}\right]} \left(\int_0^{b_0^*} [1 - \cos^l \chi] b^* db^* + \int_{b_0^*}^{B^*} [1 - \cos^l \chi] b^* db^* \right). \tag{36}$$

While the first integral is evaluated using Eq. (32), the second integral is computed as

$$\int_{b_0^*}^{B^*} [1 - \cos^l \chi] b^* db^* = \sum_{k=0}^{M-1} \frac{B^* - b_0^*}{2} w_k (1 - \cos^l \chi) \frac{(B^* - b_0^*) y_k + (B^* + b_0^*)}{2} \sqrt{1 - y_k^2}, \tag{37}$$

where y_k are the zeros of the Mth degree Chebyshev polynomial and χ is evaluated at $(((B^* - b_0^*) y_k + (B^* + b_0^*))/2, \epsilon^*)$. It can be observed that the difference in computing $S^{(l)}(\epsilon^*)$ for the exact scattering angle and the LJPA model is in the computation of the second integral.

The values of $S^{(l)}(\epsilon^*)$ are used in the computation of $W^{(l)}(n; x)$. If $x\epsilon^* = y$, Eq. (13) can be written as

$$W^{(l)}(n; x) = \frac{1}{8} \left[2 - \frac{1 + (-1)^l}{1 + l}\right] \int_0^{\infty} e^{-y} y^{n+1} S^{(l)}\left(\frac{y}{x}\right) dy. \tag{38}$$

Since the integration limits are not finite, the Gauss-Laguerre quadrature is used to compute the above integral. The integral is computed as

$$\int_0^{\infty} e^{-y} y^{n+1} S^{(l)}\left(\frac{y}{x}\right) dy = \sum_{k=1}^{N_{LG}} w_{k,n+1,N_{LG}} S^{(l)}(z_{k,n+1,N_{LG}}), \tag{39}$$

where $z_{k,n+1,N_{LG}}$ is the kth zero of the generalized Laguerre polynomial[27] of degree N_{LG}, $L_{n+1,N_{LG}}$, with the coefficients of the polynomial depending on $n + 1$, and $w_{k,n+1,N_{LG}}$ is the corresponding weight. The weights are given by[27]

$$w_{k,n+1,N_{LG}} = \frac{1}{z_{k,n+1,N_{LG}}} \frac{1}{L'^2_{n+1,N_{LG}}(z_{k,n+1,N_{LG}})}. \tag{40}$$

It should be observed that the zeros and weights used in Eq. (33) correspond to $n + 1 = 0$. For the above integration, the value of N_{LG} was fixed at 150. While the above approach works well for the collision integrals of the exact LJ scattering angle, small variations are required to compute collision integrals for the LJPA model. Since the LJPA model uses piecewise polynomial expansions, there could be small discontinuities in the value of $S^{(l)}(\epsilon^*)$ at $\epsilon^* = 0.8$, 1.0, 5.0, 20.0, and 1000.0. While these discontinuities are almost negligible, in order to ensure accurate computation of the integrals,

TABLE X. Comparison of collision integrals obtained using LJPA model with the exact values and those reported in previous works for $T^* = kT/\epsilon_{LJ} = 0.05, 0.3, 1, 10$.

	LJPA model	Exact χ	Hirschfelder *et al.*[10]	Sharipov and Bertoldo[18]
$T^* = 0.05$				
$W^{(1)}(1)$	2.4895	2.5334	...	...
$W^{(1)}(2)$	6.6366	6.7489	...	...
$W^{(2)}(2)$	5.1455	5.1889	...	...
$T^* = 0.3$				
$W^{(1)}(1)$	1.3060	1.3272	1.331	1.325
$W^{(1)}(2)$	3.3355	3.3882	3.3840	3.386
$W^{(2)}(2)$	2.8388	2.8471	2.785	2.844
$T^* = 1$				
$W^{(1)}(1)$	0.7138	0.7209	0.7197	0.720
$W^{(1)}(2)$	1.7901	1.8071	1.806	1.806
$W^{(2)}(2)$	1.5754	1.5915	1.587	1.593
$T^* = 10$				
$W^{(1)}(1)$	0.3646	0.3711	0.3712	0.3711
$W^{(1)}(2)$	1.0350	1.0512	1.0520	1.0512
$W^{(2)}(2)$	0.8065	0.8244	0.8242	0.8244

we split the integral in Eq. (38) as

$$\int_0^\infty I(y)dy = \int_0^{0.8} I(y)dy + \int_{0.8}^{1} I(y)dy + \int_1^5 I(y)dy + \int_5^{20} I(y)dy + \int_{20}^{1000} I(y)dy + \int_{1000}^{\infty} I(y)dy. \quad (41)$$

While the first 5 integrals are computed using Gauss-Chebyshev quadrature (due to finite integration limits), the last integral is computed using Gauss-Laguerre quadrature. Each Gauss-Chebyshev integration used 320 integration points and the Gauss-Laguerre integration used 150 integration points.

IV. RESULTS AND DISCUSSION

In this section, the collision integrals computed for the LJPA model and the exact scattering angle computed using the integration techniques described earlier are compared with each other and with those obtained using the GSS model which is the purely repulsive model that reproduces transport coefficients of the LJ potential. Table X shows a comparison of various collision integrals corresponding to $kT/\epsilon_{LJ} = 0.05$, 0.3, 1.0, and 10.0 for the LJPA model, exact LJ scattering angle, and previous works reported by Hirschfelder *et al.*[10] and Sharipov and Bertoldo.[18] It can be seen that the collision integrals computed using the exact scattering angles computed in this work agree extremely well with the values presented in the previous works. The reason for slight discrepancy in the $W^2(2)$ value at $kT/\epsilon_{LJ} = 0.3$ presented by Hirschfelder *et al.*[10] is not clear particularly due to the good agreement of other collision integrals. The exact values obtained in this work are in good agreement with those reported by Sharipov and Bertoldo.[18] The LJPA model shows very good agreement with the exact value with the errors for all kT/ϵ_{LJ} being within 3% for the reported values.

A. Cross sections $S^{(l)}(\epsilon^*)$

In order to perform detailed comparisons, the variation of the cross sections $S^{(1)}$, $S^{(2)}$, $S^{(3)}$, and $S^{(4)}$ for the LJPA model, exact LJ scattering angle, and the GSS model are compared in Figure 1. The functional forms of $S^{(l)}$ for $l = 1$, 2, 3, and 4 using Eq. (11) and the scattering angle relation for

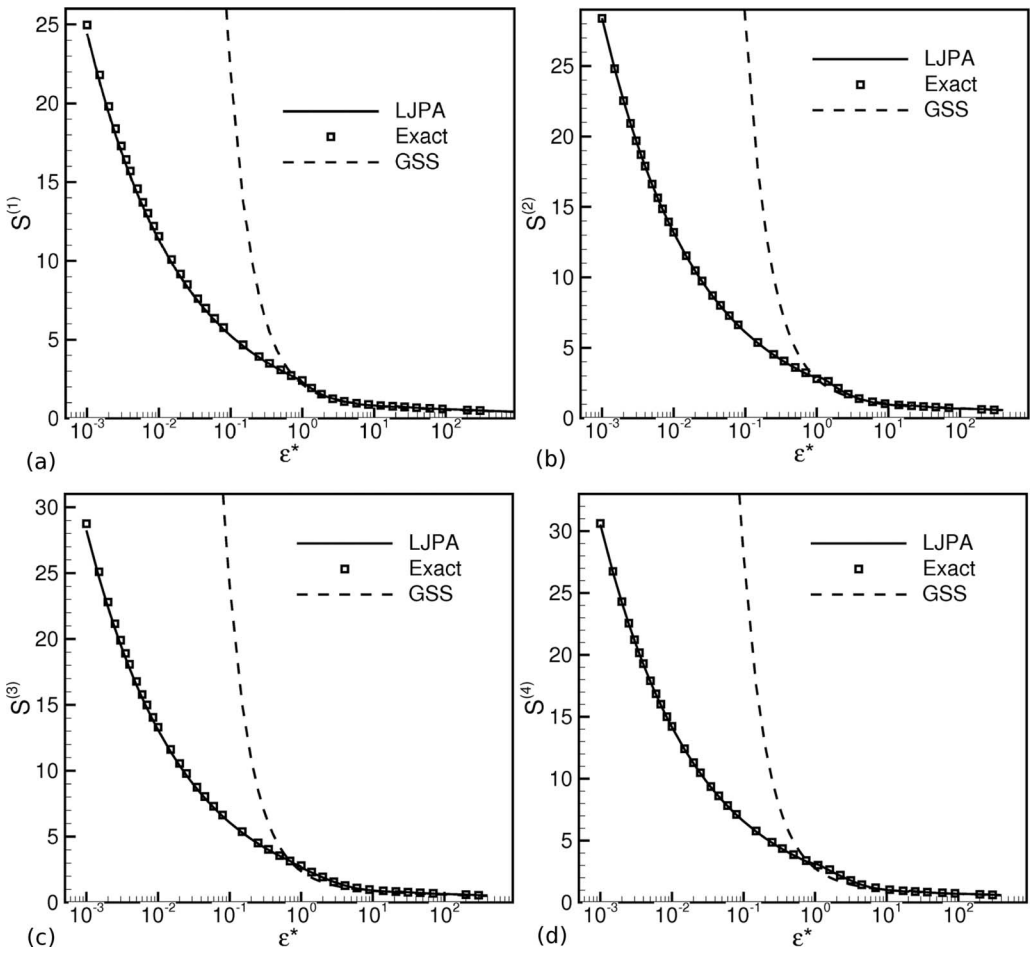

FIG. 1. Comparison of cross sections (a) $S^{(1)}$, (b) $S^{(2)}$, (c) $S^{(3)}$, and (d) $S^{(4)}$ for the LJPA model, exact LJ scattering, and the GSS model.

the GSS model are given by

$$S^{(1)}_{\mathrm{GSS}}(\epsilon^*) = \frac{2}{\pi(\alpha+1)}(3.962\epsilon^{*-0.133} + 4.558\epsilon^{*-1.25}), \tag{42}$$

$$S^{(2)}_{\mathrm{GSS}}(\epsilon^*) = \frac{6\alpha}{\pi(\alpha+1)(\alpha+2)}(3.962\epsilon^{*-0.133} + 4.558\epsilon^{*-1.25}), \tag{43}$$

$$S^{(3)}_{\mathrm{GSS}}(\epsilon^*) = \frac{2(3\alpha^2+3\alpha+6)}{\pi(\alpha+1)(\alpha+2)(\alpha+3)}(3.962\epsilon^{*-0.133} + 4.558\epsilon^{*-1.25}), \tag{44}$$

$$S^{(4)}_{\mathrm{GSS}}(\epsilon^*) = \frac{10(\alpha^3+3\alpha^2+8\alpha)}{\pi(\alpha+1)(\alpha+2)(\alpha+3)(\alpha+4)}(3.962\epsilon^{*-0.133} + 4.558\epsilon^{*-1.25}). \tag{45}$$

For GSS, $\alpha = 1.5$ and is independent of the gas species. The comparison shows that for values of $\epsilon^* > 1$, the agreement between the GSS model and the exact LJ scattering angle is excellent. However, the GSS model leads to a rapid increase in all cross sections for values of $\epsilon^* \leq 1$. This is a direct consequence of the rapid divergence of the GSS total cross section, σ_T as mentioned in Sec. I

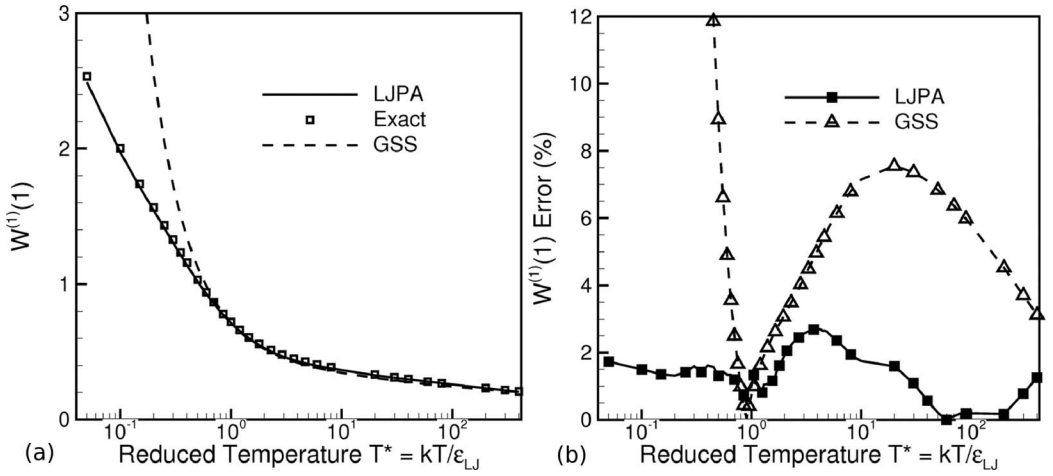

FIG. 2. Comparison of collision integral (a) $W^{(1)}(1)$ for the LJPA model, exact LJ scattering, and the GSS model along with the (b) corresponding errors.

B. Collision integrals $W^{(l)}(n)$

The cross sections $S^{(l)}$ are used to compute the collision integrals $W^{(l)}(n)$ which are used to obtain the viscosity and diffusion coefficients using Chapman-Enskog theory.[20] Figure 2 shows a comparison of the collision integral $W^{(1)}(1)$ obtained using the LJPA model, GSS model, and the exact LJ collision integral computed in this work for the reduced temperature range $0.05 \leq kT/\epsilon_{\mathrm{LJ}} \leq 400$. $W^{(1)}(1)$ is the collision integral that is used to compute the first approximation of the self-diffusion coefficient using the Chapman-Enskog theory. In order to quantify the errors for the LJPA model and the GSS model, the errors are also shown as a function of the reduced temperature. The LJPA model error is obtained as

$$\Delta^{(1)}(1)_{\mathrm{LJPA}} = \frac{|W^{(1)}(1)_{\mathrm{LJPA}} - W^{(1)}(1)_{\mathrm{Exact\ LJ}}|}{W^{(1)}(1)_{\mathrm{Exact\ LJ}}}. \tag{46}$$

Since the GSS model was constructed using the tabulated collision integral values by Hirschfelder *et al.*,[10] the error for the GSS model is obtained as

$$\Delta^{(1)}(1)_{\mathrm{GSS}} = \frac{|W^{(1)}(1)_{\mathrm{GSS}} - W^{(1)}(1)_{\mathrm{Hirschfelder\ \textit{et al.}}}|}{W^{(1)}(1)_{\mathrm{Hirschfelder\ \textit{et al.}}}}. \tag{47}$$

It should be mentioned that the values reported by Hirschfelder *et al.*[10] and the values computed using the exact scattering angle in this work are in good argument. For $W^{1}(1)$, the maximum difference is 0.7% (at $\epsilon^* = 400$) and the average difference is 0.1%. The $W^{1}(1)$ computed using the LJPA model agrees with the exact value within 4% for the entire range of reduced temperature values considered. The LJPA model almost always leads to an underprediction of the collision integral which is partly due to neglection of collisions with $\chi < 0.1$ radian. This deviation is a maximum for $l = 1$ since $(1 - \cos^{l}0.1)$ is maximum when $l = 1$. On the other hand, the $W^{(1)}(1)$ computed using the GSS model leads to slightly larger errors, as mentioned by Kim *et al.*[22] for almost all values of $kT/\epsilon_{\mathrm{LJ}}$ with the error being maximum for the lowest $kT/\epsilon_{\mathrm{LJ}}$. This does not come as a surprise since the GSS model was completely based on the values of $W^{2}(2)$ and the agreement is surprisingly good considering that it was not formulated using $W^{(1)}(1)$ values. Figure 3 shows the comparison between the LJPA, GSS models, and the exact value of $W^{1}(2)$. The trend is similar to the results obtained for $W^{(1)}(1)$ with the GSS error being, in general, larger than the LJPA error and, in particular, the low temperature performance of the GSS is not very good.

Figure 4 shows the results for the collision integral $W^{(2)}(2)$ and except for low reduced temperatures, the performance of GSS is comparable and in some cases better than the LJPA model. The LJPA model deviation from the exact value of the collision integral continues to be within 4%. The collision integral $W^{2}(2)$ is used to compute the viscosity and the underprediction of around 2–3% in

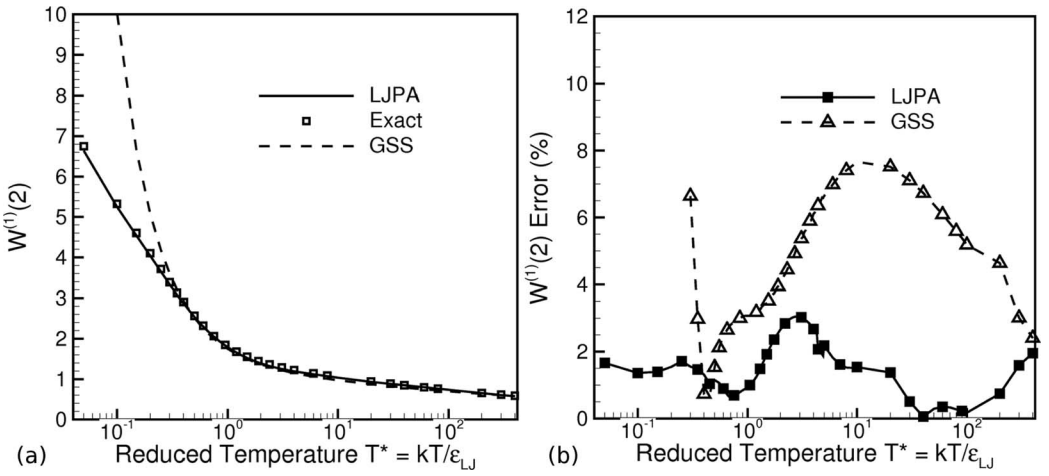

FIG. 3. Comparison of collision integral (a) $W^{(1)}(2)$ for the LJPA model, exact LJ scattering, and the GSS model along with the (b) corresponding errors.

viscosity at around $\epsilon^* = 2.5$ predicted by theory was also observed in DSMC simulations performed using the LJPA model[19] for argon at 273 K. Figure 5 shows the corresponding results for $W^{(2)}(4)$ and $W^{(2)}(5)$ with the trends being similar to $W^{(2)}(2)$. Figure 6 shows similar comparisons for collision integrals corresponding to higher values of $l = 3$ and l=4. For l=4, the collision integral $W^{(4)}(4)$ is chosen because it is tabulated by Hirschfelder[10] and hence enables comparison of the GSS model with those tabulated values. For l=3, there are no collision integrals tabulated by Hirschfelder *et al.*[10] and hence $W^3(1)$ was chosen.

The agreement between the exact LJ collision integrals and the LJPA model is excellent once again with the maximum error being about 2.8% for $W^{(3)}(1)$ and 3.7% for $W^{(4)}(4)$. For the GSS model, the errors were computed only for $0.3 \leq kT/\epsilon_{LJ} \leq 400$ since the error is very high outside this range. For $W^{(4)}(4)$, the maximum error using GSS model is about 20% with the error being greater than 8% for $kT/\epsilon_{LJ} \leq 1.25$. On the other hand, for $W^{(3)}(1)$, the maximum error using GSS model is about 22% with the error being greater than 8% for $kT/\epsilon_{LJ} \leq 90$. Other values of n have not been reported here for $l = 3$ and $l = 4$ but the error trends were very similar.

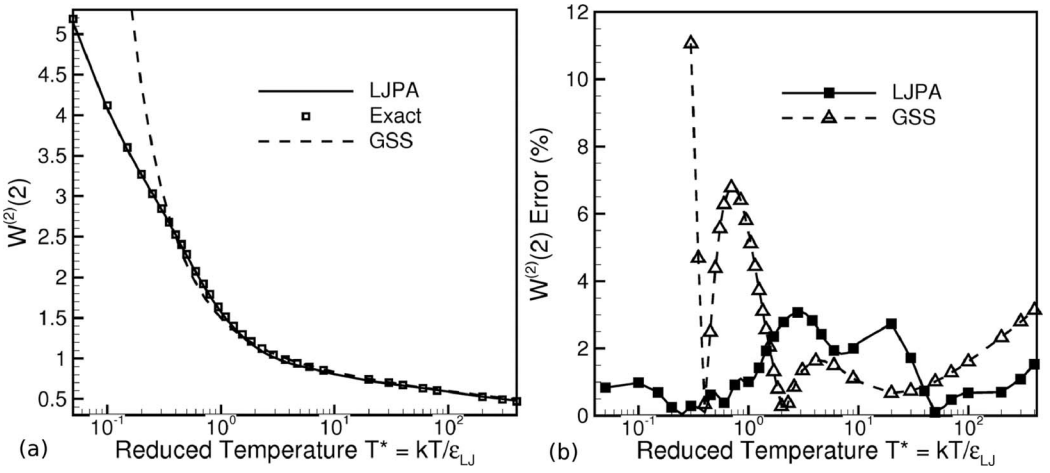

FIG. 4. Comparison of collision integral (a) $W^{(2)}(2)$ for the LJPA model, exact LJ scattering, and the GSS model along with the (b) corresponding errors.

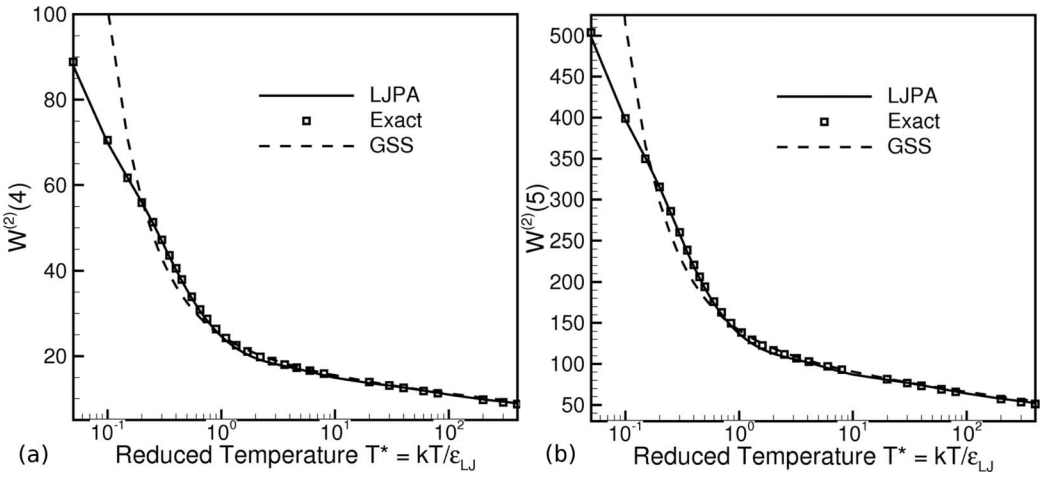

FIG. 5. Comparison of collision integrals (a) $W^{(2)}(4)$ and (b) $W^{(2)}(5)$ for the LJPA model, exact LJ scattering, and the GSS model.

C. Transport coefficients

It is important to put the results obtained using the LJPA model in perspective by using the collision integrals to compute the first approximations of the self-diffusion coefficient and the viscosity of argon. The first approximation of the self-diffusion coefficient based on the Chapman-Enskog theory is given by[20]

$$[D]_1 = \frac{3}{16 n \sigma_{\mathrm{LJ}}^2 W^{(1)}(1)} \sqrt{\frac{kT}{\pi m}} \tag{48}$$

and the first approximation of the viscosity coefficient is given by[20]

$$[\mu]_1 = \frac{5}{16 \sigma_{\mathrm{LJ}}^2 W^{(2)}(2)} \sqrt{\frac{kmT}{\pi}}. \tag{49}$$

Figure 7 shows a comparison of the transport coefficients, i.e., viscosity and self-diffusion, for argon obtained using various purely repulsive DSMC molecular along with the LJPA model and a compilation[28] based on a large set of experimental data. It can be seen that both GSS and LJPA models agree with the compilation based on experiments but the GSS model starts to deviate significantly

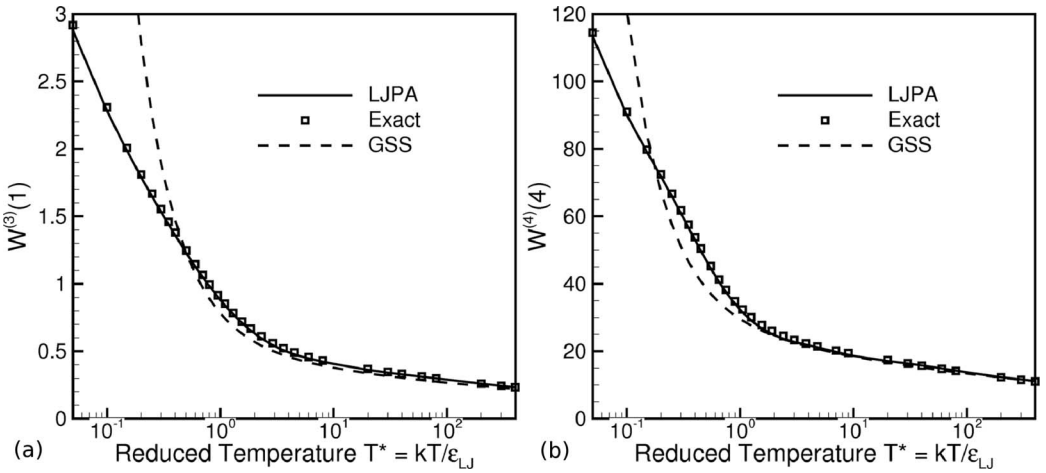

FIG. 6. Comparison of collision integrals (a) $W^{(3)}(1)$ and (b) $W^{(4)}(4)$ for the LJPA model, exact LJ scattering, and the GSS model

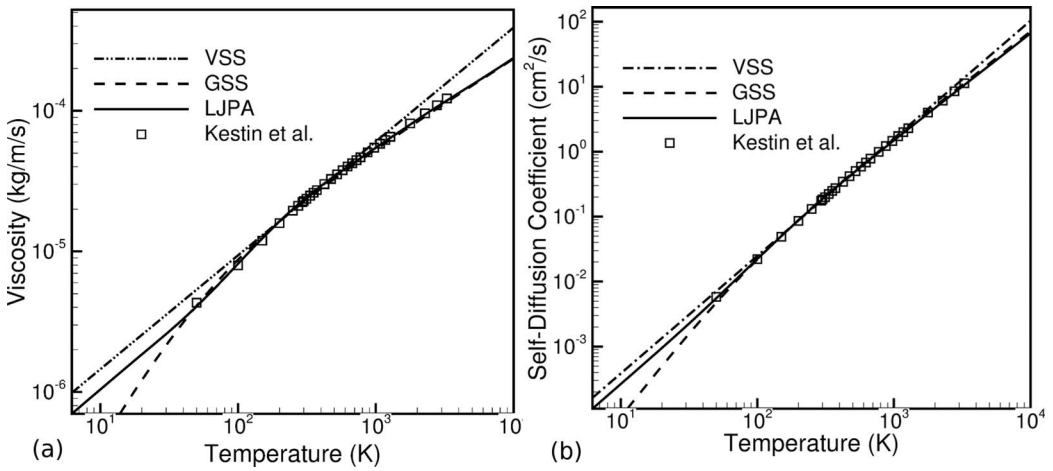

FIG. 7. Comparison of argon (a) viscosity and (b) self-diffusion coefficient using the LJPA model, GSS model, VHS model, and compilation of experiments by Kestin *et al.*[28]

from the LJPA model at about 50 K and the difference increases as the temperature is decreased. The potential well depth of argon is $\epsilon_{LJ}/k = 124$ K and hence the GSS model viscosity deviates from LJPA viscosity at relatively low temperatures. However, the potential well depth depends on the gas under consideration and Table I showed that certain gases, such as metal vapors, have a significantly deeper LJ potential well. For these gases, the large deviation of the GSS model from LJPA model occurs even at moderate temperatures. Also, since the LJPA model uses the scattering angle information of the LJ potential, using it in DSMC would provide solutions, including velocity distribution functions (and hence energy distribution functions) of molecules, that agree well with MD simulations as long as multi-body collisions can be neglected. One example of an application that would require the accurate energy distribution of molecules is in multiscale simulations of thin film deposition processes where prediction of the microstructure of these films depends on the energies of vapor molecules arriving at the growth location. In these cases, reproducing viscosity coefficient would lead to accurate prediction of only the number flux of molecules and hence only the thickness of the thin films. On the other hand, a model such as the proposed LJPA model will reproduce the collision dynamics better thereby leading to a better prediction of the energy (or velocity) distribution of the molecules and hence the microstructure of the thin films. The LJPA model is also an ideal model for use with hybrid MD/DSMC methods, similar to those reported by Gu *et al.*,[21] since MD methods are typically based on the LJ intermolecular potential between molecules.

V. CONCLUSIONS

A Lennard-Jones binary scattering model obtained by representing the exact scattering angle as a polynomial expansion in the two non-dimensional collision variables is considered. Rigorous theoretical verification of the model is performed by comparing various collision quantities such as the diffusion, viscosity cross sections, and the collision integrals obtained using them. The quantities compared included $S^{(l)}$ for $1 \leq l \leq 4$ and $W^{(1)}(1)$, $W^{(1)}(2)$, $W^{(2)}(2)$, $W^{(2)}(4)$, $W^{(2)}(5)$, $W^{(3)}(1)$, and $W^{(4)}(4)$. The collision integrals obtained using the LJPA model agree extremely well, within 3.5%, with the collision quantities of the exact LJ scattering angle for the entire range of reduced temperatures between 0.05 and 400 showing that the polynomial expansion based model is a good representation of the exact LJ scattering. The LJPA model was also compared with the GSS model which is the closest in terms of fidelity among the existing DSMC collision models to study the differences between the two models. While the GSS model's performance for the collision integral used in the first approximation of the viscosity coefficient is comparable to the LJPA model for most of the reduced temperatures considered, the collision integral used to obtain the first approximation of the diffusion coefficient leads to larger errors around 8% for certain reduced temperatures. The

viscosity and diffusion cross sections of the GSS model itself deviate from the LJPA model for reduced collision energies less than 1.0 which is important when reproducing only bulk transport coefficients is insufficient. The GSS collision integrals corresponding to larger values of $l = 3$ and 4 lead to larger deviation from the exact LJ scattering values with maximum errors around 20%. The low reduced temperature performance of the LJPA model is also very good making it useful for the non-equilibrium simulations of flows of gases such as metal vapors that have a deep potential well. In summary, the LJPA model while retaining all the advantages of the GSS model also reproduces the binary collision dynamics of the LJ potential in great detail. The LJPA model being based on the scattering angle as opposed to viscosity or diffusion coefficients is likely to agree most closely with MD simulations when compared to other existing DSMC collision models and therefore is well suited for hybrid MD/DSMC simulations.

[1] G. A. Bird, *Molecular Gas Dynamics and the Direct Simulation of Gas Flows*, 2nd ed. (Oxford University Press, New York, 1994).
[2] F. Cheremisin, "Numerical methods for the direct solution of the kinetic boltzmann equation," USSR Comput. Math. Math. Phys. **25**, 156 (1985).
[3] S. Yen, "Numerical solution of the nonlinear Boltzmann equation for nonequilibrium gas flow problems," Annu. Rev. Fluid Mech. **16**, 67 (1984).
[4] Z. Tan, Y. K. Chen, P. L. Varghese, and J. L. Howell, "New numerical strategy to evaluate the collision integral of the Boltzmann equation," *Rarefied Gas Dynamics: Theoretical and Computational Techniques*, AIAA, Washington DC (1989), p. 359.
[5] V. Aristov, *Direct Methods for Solving the Boltzmann Equation and Study of Nonequilibrium Flows* (Springer, Netherlands, 2001).
[6] G. Bird, "Approach to translational equilibrium in a rigid sphere gas," Phys. Fluids **6**, 1518 (1963).
[7] K. Koura and H. Matsumoto, "Variable soft sphere molecular model for inverse-power-law or Lennard-Jones potential," Phys. Fluids A: Fluid Dyn. **3**, 2459 (1991).
[8] H. Hassan and D. Hash, "A generalized hard-sphere model for Monte Carlo simulation," Phys. Fluids A: Fluid Dyn. **5**, 738 (1993).
[9] J. Fan, "A generalized soft-sphere model for Monte Carlo simulation," Phys. Fluids **14**, 4399 (2002).
[10] J. O. Hirschfelder, R. B. Bird, and E. L. Spotz, "The transport properties for non-polar gases," J. Chem. Phys. **16**(10), 968 (1948).
[11] R. Bird, W. Stewart, and E. Lightfoot, *Transport Phenomena* (Wiley, New York, 2004).
[12] G. Pham-Van-Diep, D. Erwin, and E. Muntz, "Nonequilibrium molecular motion in a hypersonic shock wave," Science **245**, 624 (1989).
[13] J. Lengrand, J. Allegre, A. Chpoun, and M. Raffin, "Rarefied hypersonic flow over a sharp flat plate- numerical and experimental results," Rarefied Gas Dyn.: Space Sci. Eng. **160**, 276 (1994).
[14] M. Holden, "Development and code evaluation studies in hypervelocity flows in the LENS facility," in *Aerothermodynamics for Space Vehicles*, European Space Agency, Paris, France (1995), Vol. 367, p. 319.
[15] D. Smith, *Thin-Film Deposition: Principles and Practice* (McGraw-Hill, New York, 1995).
[16] R. Farrow, *Molecular Beam Epitaxy: Applications to Key Materials* (Noyes Publications, New Jersey, 1995).
[17] F. Tcheremissine, "Solution to the Boltzmann kinetic equation for high-speed flows," Comput. Math. Math. Phys. **46**, 315 (2006).
[18] F. Sharipov and G. Bertoldo, "Numerical solution of the linearized Boltzmann equation for an arbitrary intermolecular potential," J. Comput. Phys. **228**, 3345 (2009).
[19] A. Venkattraman and A. Alexeenko, "DSMC collision model for the Lennard-Jones potential: Efficient algorithm and verification," in *Proceedings of the 42nd AIAA Thermophysics Conference, AIAA, 2011-3313* (AIAA, Honolulu, Hawaii, 2011).
[20] S. Chapman and T. Cowling, *The Mathematical Theory of Non-Uniform Gases: An Account of the Kinetic Theory of Viscosity, Thermal Conduction and Diffusion in Gases* (Cambridge University Press, Cambridge, England, 1990).
[21] K. Gu, C. Watkins, and J. Koplik, "Atomistic hybrid DSMC/NEMD method for nonequilibrium multiscale simulations," J. Comput. Phys. **229**, 1381 (2010).
[22] J. Kim, O. Kwon, and C. Park, "Modification and expansion of the generalized soft-sphere model to high temperature based on collision integrals," Phys. Fluids **20**, 017105 (2008).
[23] P. Valentini and T. E. Schwartzentruber, "Large-scale molecular dynamics simulations of normal shock waves in dilute argon," Phys. Fluids **21**, 066 (2009).
[24] H. Matsumoto and K. Koura, "Comparison of velocity distribution functions in an argon shock wave between experiments and Monte Carlo calculations for Lennard-Jones potential," Phys. Fluids A: Fluid Dyn. **3**, 30 (1991).
[25] J. O. Hirschfelder, C. F. Curtiss, and R. B. Bird, *Molecular Theory of Gases and Liquids* (Wiley, New York, 1954).
[26] A. Venkattraman and A. Alexeenko, "Direct simulation Monte Carlo modeling of e-beam metal deposition," J. Vac. Sci. Technol. A **28**, 916 (2010).
[27] P. Rabinowitz and G. Weiss, "Tables of abscissas and weights for numerical evaluation of integrals of the form $\int_0^\infty e^{-x} x^n f(x) dx$," Math. Tables Aids Comput. **13**, 285 (1959).
[28] J. Kestin, K. Knierim, E. A. Mason, B. Najafi, S. T. Ro, and M. Waldman, "Equilibrium and transport properties of the noble gases and their mixtures at low density," J. Phys. Chem. Ref. Data **13**, 229 (1984).